Superactivity of MOF-808 towards peptide bond hydrolysis

Hong Giang T. Ly, Guangxia Fu, Aleksandar Kondinski, Bart Bueken, Dirk De Vos, and Tatjana N. Parac-Vogt

J. Am. Chem. Soc., **Just Accepted Manuscript** • DOI: 10.1021/jacs.8b01902 • Publication Date (Web): 23 Apr 2018

Superactivity of MOF-808 towards peptide bond hydrolysis

Hong Giang T. Ly,[a] Guangxia Fu,[b] Aleksandar Kondinski,[a] Bart Bueken,[b] Dirk De Vos,* [b] and Tatjana N. Parac-Vogt* [a]

[a] Laboratory of Bioinorganic Chemistry, Department of Chemistry, KU Leuven, Celestijnenlaan 200F, 3001 Leuven, Belgium

[b] Centre for Surface Chemistry and Catalysis, KU Leuven, Celestijnenlaan 200F, 3001 Leuven, Belgium

ABSTRACT: MOF-808, a Zr(IV)-based metal-organic framework, has been proven to be a very effective heterogeneous catalyst for the hydrolysis of the peptide bond in a wide range of peptides and in hen egg white lysozyme protein. The kinetic experiments with a series of Gly-X dipeptides with varying nature of amino acid side chain have shown that MOF-808 exhibits selectivity depending on the size and chemical nature of the X side chain. Dipeptides with smaller or hydrophilic residues were hydrolyzed faster than those with bulky and hydrophobic residues that lack electron rich functionalities which could engage in favourable intermolecular interactions with the btc linkers. Detailed kinetic studies performed by ^{1}H NMR spectroscopy revealed that the rate of glycylglycine (Gly-Gly) hydrolysis at pD 7.4 and 60 °C was 2.69×10^{-4} s^{-1} ($t_{½}$ = 0.72 h), which is more than four orders of magnitude faster compared to the uncatalyzed reaction. Importantly, MOF-808 can be recycled several times without significantly compromising the catalytic activity. A detailed quantum-chemical study combined with experimental data allowed to unravel the role of the $\{Zr_6O_8\}$ core of MOF-808 in accelerating Gly-Gly hydrolysis. A mechanism for the hydrolysis of Gly-Gly by MOF-808 is proposed in which Gly-Gly binds to two Zr(IV) centers of the $\{Zr_6O_8\}$ core via the oxygen atom of the amide group and the N-terminus. The activity of MOF-808 was also demonstrated towards the hydrolysis of hen egg white lysozyme, a protein consisting of 129 amino acids. Selective fragmentation of the protein was observed with 55% yield after 25 hours under physiological pH.

INTRODUCTION

In the quest for new efficient and selective artificial proteases, which are of great importance for protein structure analysis, protein engineering, and target-specific protein-cleaving drug design,[1] efforts have been directed to using metal ions or metal complexes as Lewis-acid catalysts for cleaving proteins into suitable fragments with restored carboxylic and amine functional groups. However, this is a challenging task due to the extreme inertness of the peptide bond, which exhibits an estimated half-life of up to 350 years under physiological pH and temperature.[2] Certain salts of lanthanides and transition metals can enhance the rate of peptide bond hydrolysis at neutral pH.[3] However, the main limitation of such approach is the formation of gels at neutral and basic pH conditions, which is often observed for many transition metal and lanthanide ions, especially for Ce(IV) and Zr(IV). Efforts to avoid gel formation have been made by adding organic ligands to form metal complexes.[4] Several metal complexes of Ce(IV),[5] Zr(IV),[4] Co(III),[6] Cu(II),[7] Zn(II),[3, 8] Pd(II),[9] and Ni(II)[10] have been reported to promote the hydrolysis of amide bonds in a wide range of peptides and proteins. Complexes of Cu(II) have been shown to hydrolyze the X-Ser(Thr) bond in X-Ser(Thr)-His sequences, but their reactivity was lost at physiological conditions due to the formation of strong metal-amide nitrogen bonds resulting in catalytically inactive complexes.[11] Moreover, complexes of Pt(II) and Pd(II) only selectively hydrolyzed at Met and His residues at low pH values, typically below pH 2.[9b, 12]

In our efforts towards developing novel artificial peptidases, we have recently focused our attention on the use of metal-substituted polyoxometalate (POM) complexes. We have shown that a series of Zr(IV)-substituted Lindqvist-, Keggin-, and Wells-Dawson-type POMs efficiently hydrolyze unactivated peptide bonds in dipeptides and oligopeptides.[13] The superior reactivity of Zr(IV) over other metals including Mn(III), Fe(III), Co(II), Ni(II), Cu(III), Y(III), La(III), Eu(III) or Yb(III) substituted in POMs has been explained by the large coordination numbers, flexible geometries, oxophilicity and increased Lewis acidity of Zr(IV).[13a] The reaction mechanism for peptide bond hydrolysis in these systems has been investigated in detail. The reactions were significantly accelerated by formation of hydrolytically active complexes in which the amine nitrogen and amide oxygen atoms coordinate to Zr(IV), polarizing the peptide bond and making it more susceptible for nucleophilic attack by water. In addition, the reactions were also assisted by the presence of the C-terminal carboxylate group which abstracts a proton from the attacking water molecule, assisting the nucleophilic attack of a solvent water molecule on the amide carbonyl carbon.[14] The study of the catalytic activity of Zr(IV)-POMs was expanded to the hydrolysis of proteins such as insulin chain B, ovalbumin, hen egg white lysozyme, human serum albumin, myoglobin and hemoglobin.[15] Highly selective hydrolysis occurring mainly upstream from aspartate residues was achieved. In addition to the direct binding to the amide carbonyl oxygen, which results in activation of the peptide bond towards hydrolysis, the negatively charged Zr(IV)-substituted POMs were found to electrostatically interact with positively charged patches on the protein surface, resulting in selective hydrolysis of proteins in mildly acidic and neutral media.

Despite the remarkable ability of Zr(IV)-substituted POMs to cleave peptide bonds, catalyst recycling and product purification remain problematic. The catalysts often cause formation of precipitates in the reaction mixture, thereby preventing the use of mass spectrometric techniques to identify fragmentation patterns. Furthermore, the Zr(IV)-substituted POMs undergo complex equilibria in solution, often resulting in formation of catalytically inactive dimers. Therefore, the development of heterogeneous catalysts that are able to hydrolyze peptide bonds and can be easily removed from the reaction mixtures and recycled, would greatly advance the potential of using artificial metalloenzymes in the fields of proteomics and biotechnology.

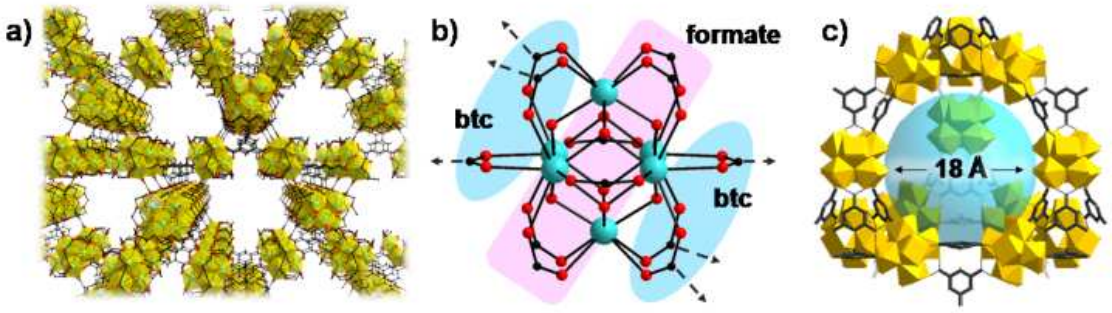

Figure 1. Combined ball-and-stick and polyhedral representation of MOF-808 (a), its functional $[Zr_6O_4(OH)_4]$ cluster sandwiched between formate and btc ligands (b) and the primary pore (c). Color code: Zr = blue, O = red, C = black, $\{ZrO_8\}$ = yellow polyhedra. Hydrogen atoms have been omitted for clarity.

Metal–organic frameworks (MOFs) are a class of hybrid inorganic–organic microporous crystalline materials, which consist of metal ions with bridging organic linkers.[16] The appropriate combination of organic linkers and metal clusters can result in an almost infinite number of MOFs containing catalytically active sites located inside the porous framework with controlled pore sizes.[17] Owing to their fascinating structures and unique properties such as nanoscale porosity, high surface area, good thermal stability, and uniformly structured cavities, MOFs hold great potential for a wide range of applications, especially in catalysis.[18] The incorporation of Lewis acidic Zr(IV) ions into hybrid frameworks forms various Zr-carboxylate MOFs such as UiO-66, MOF-808, and NU-1000.[19] The Lewis-acid catalytic activity of these Zr-MOFs has been exploited e.g. for the hydrolysis of phosphate ester bonds and the citronellal cyclization.[20] These studies showed excellent catalytic performance of Zr-MOFs; however, to the best of our knowledge there is only one recent report in which hydrolysis of a protein has been achieved in the presence of a MOF, viz. HKUST-1 or $[Cu_3(btc)_2]$(btc= benzene-1,3,5-tricarboxylate).[21] However, the authors reported that in the presence of a protein some of Cu(II) leached out into the solution suggesting a limited stability of HKUST-1 under condition used for protein hydrolysis.

One of the $\{Zr_6O_8\}$-cluster-based MOFs that has recently received much attention is MOF-808 ($[Zr_6O_4(OH)_4(btc)_2(HCOO)_6]$ (btc = benzene-1,3,5-tricarboxylate).[22] Similarly to other MOFs based on the $\{Zr_6O_8\}$ cluster, MOF-808 shows excellent chemical stability, but is thermally more labile due to the lower cluster connectivity as compared to for instance UiO-66. The crystal structure of MOF-808 (Figure 1a) exhibits ideally octahedral $\{Zr_6O_8\}$ cluster-type building blocks that are tetraprotonated (*i.e.* $\{Zr_6(\mu_3\text{-}O)_4(\mu_3\text{-}OH)_4\}$), capped and interconnected by six btc linkers binding in trigonal antiprism fashion (Figure 1b). The resulting MOF-808 framework features the **spn** topology and exhibits pores with a diameter 18 Å, which can allow the permeation of oligopeptides in the pores of the framework (Figure 1c).[19c, 23] The remaining sites of the eight-coordinated Zr(IV) centers are covered with terminal formate ligands that exhibit relative lability, easily leading to generation of Lewis acidic sites. These have been utilized for catalytic hydrolysis of the notorious nerve agent simulant dimethyl 4-nitrophenyl phosphate (DMNP).[20b] In addition, Klempere and coworkers have reported that the formate ligands can be selectively displaced from MOF-808 by sulfate moieties to generate its sulfated analogue which is catalytically active in various acid-catalyzed reactions including Friedel–Crafts acylation, esterification, and isomerization.[24]

The high stability of the $\{Zr_6O_8\}$-connector brick and its coverage with formate ligands were our first motivation to investigate in detail the reactivity of MOF-808 towards the hydrolysis of peptide bonds in a series of dipeptides. The effects of pH, temperature, and inhibitors on the hydrolysis rate are investigated. In addition, the effects of the amino acid side chains on the hydrolysis of dipeptides containing a glycine (Gly) residue at the N-terminus (Gly-X) by MOF-808 are explored. Due to the highly stable molecular Keplerate which is a promising candidate to remain intact during the catalytic process, highly oxophilic sites which can be used to coordinate a dipeptide moiety as well as the unsaturated coordination of the Zr(IV) ion, we envisioned that MOF-808 could be a stable and superior catalyst for peptide bond hydrolysis. Insights into the preferable binding modes that allow activation of the peptide hydrolysis were obtained by molecular modeling and DFT calculations. Finally, the ability of MOF-808 to selectively cleave peptide bonds in a protein under

neutral pH has been also demonstrated.

EXPERIMENTAL SECTION

Materials

N,N-Dimethylformamide (DMF), 1,3,5-benzenetricarboxylic acid (H_3btc), formic acid, acetic acid, anhydrous methanol, anhydrous acetone, chloroform, acetonitrile, ethanol and diethyl ether were obtained from Acros Organics. D_2O, DCl, NaOD, $ZrOCl_2{\cdot}8H_2O$, dipeptides, hen egg white lysozyme (HEWL), dicarboxylic acids (oxalic, malonic, succinic, glutaric, adipic, and malic acid), and citric acid were purchased from Sigma-Aldrich. All chemicals were purchased as pure reagent grades and used without further purification.

Synthesis of MOF-808 and molecular Zr_6-clusters

MOF-808 was prepared solvothermally by heating solutions containing zirconium salt, the acid form of the organic linker and formic acid as modulating agent, as described in literature with some modifications.[22] Typically, H_3btc (3.75 mmol, 0.786 g) and $ZrOCl_2{\cdot}8H_2O$ (3.75 mmol, 1.209 g) were mixed in DMF (150 mL) and formic acid (150 mL). The mixture was placed in a closed 1-L Schott DURAN bottle, which was heated at 130 °C for 48 h. Following synthesis, the obtained white powder was washed by DMF twice per day for three days, followed by washing with methanol twice per day for three days and collected by centrifugation. The MOF-808 was activated at 150 °C for 20 h before performing experiments. The zirconium benzoate ($Zr_6(OH)_4O_4(OBz)_{12}(PrOH){\cdot}4BzOH$) and zirconium methacrylate ($Zr_6(OH)_4O_4(OMc)_{12}(PrOH){\cdot}3McOH$) clusters were synthesized following the procedures described in literature.[25]

Peptide bond hydrolysis studies

The hydrolyses were performed at pD 7.4 and 60 °C. To a solid sample of MOF-808 (3.1 mg, 2.0 μmol) in a glass vial was added 950 μL of D_2O; this was stirred at room temperature for 30 min to finely disperse the MOF particles. To the suspension was then added peptide (50 μL of 40 mM peptide, 2.0 μmol of peptide). The reaction mixture was adjusted to pD 7.4 with NaOD and was kept at 60 °C. After different time increments, the reaction mixture was centrifuged at 15000 rpm for 20 min to remove the MOF. To the solution was added 3-(trimethylsilyl) propionic-2,2,3,3-d4 acid sodium salt (TMSP-d_4) before recording ^{1}H NMR spectra. The effect of MOF-808 amounts ranging from 0.5 μmol to 10.0 μmol on the hydrolysis of 2.0 mM Gly-Gly was studied in a similar way.

To study the effect of mono-, di- and tricarboxylic acids as inhibitors on the hydrolysis of Gly-Gly by MOF-808 at pD 7.4 and 60 °C, reaction mixtures containing 3.1 mg of MOF-808, 2.0 μmol of Gly-Gly, and 10.0 μmol of monocarboxylic acids or 5.0 μmol of the other acids were adjusted to pD 7.4 with NaOD and kept at 60 °C for 2h.

The observed reaction rate constants were obtained by fitting peptide concentrations to a first-order decay function.

Protein hydrolysis studies

The hydrolysis of HEWL (0.02 mM) by MOF-808 (3.1 mg) was performed in phosphate buffer (pH 7.4). Samples were stirred and incubated at 37 °C and 60 °C and aliquots were taken at different time increments and analyzed by SDS-PAGE.

Electrophoresis

SDS-PAGE was performed on a 4% (w/v) polyacrylamide gel in 0.5 M Tris-HCl buffer pH 6.8 stacking gel and a 16% (w/v) polyacrylamide in 1.5 M Tris-HCl buffer pH 8.8 resolving gel. Samples (15 μL) were supplemented with 5 μL of sample buffer and heated at 100 °C for 5 min, followed by loading 10 μL of the resulting solution on the gel. Page Ruler unstained low range protein ladder was used as a molecular mass standard. An OmniPAGE electrophoretic cell was combined with an EV243 power supply (both produced by Consort, Turnhout, Belgium). Experiments were performed at 200 V for 1.5 h.

Gel image analysis

Proteins in SDS-PAGE gels were visualized with silver staining and an image of each gel was taken using a Gel Doc EZ Imager (Bio-Rad, Hercules, CA). The band percentage of the fragments was determined with the Bio-Rad Image Lab software.

Adsorption studies

The adsorption was carried out at pD 7.4 and room temperature. To solid samples of MOF-808 (3.1 mg, 2.0 μmol) in glass vials was added D_2O; these mixtures were stirred at room temperature for 30 min to finely disperse the MOF particles. To the suspensions were then added 40 mM Gly-Gly to have 1 mL-mixtures containing 2.0 μmol of MOF-808 and 0.5 to 50.0 μmol of Gly-Gly. The mixtures were adjusted to pD 7.4 with NaOD and were kept at room temperature. After a certain time, the mixtures were centrifuged to remove the MOF before recording ^{1}H NMR spectra.

Recycling experiments

In order to test the recyclability of MOF-808 as a catalyst for peptide bond hydrolysis, Gly-Gly hydrolysis was repeated five times starting from one batch of catalyst in a glass vial. After each run, the vial was centrifuged to separate the solution containing the unreacted substrate Gly-Gly and the hydrolyzed products (Gly and cyclic Gly-Gly). H_2O was added to the vial and stirred for 1 h and subsequently centrifuged to remove H_2O. This process was repeated four times. Next, the material was stirred in an organic solvent (methanol, acetone, chloroform, acetonitrile, ethanol, diethyl ether, or *N,N*-dimethylformamide) for 1 day to exchange water. This process was repeated twice and the used MOF-808 was air dried and activated at 150 °C for 20 h. Subsequently, the catalysis was repeated as described above.

Measurements

Solution ^{1}H NMR spectra were recorded on a Bruker Avance 400 spectrometer and TMSP-d_4 was used as an internal reference. Powder X-ray Diffraction (PXRD) was performed on a STOE STADI P Combi instrument in Debye-Scherrer geometry (Cu Kα1) using an IP position-

sensitive detector (2θ = 0-60°; Δ2θ = 0.03°). Fourier transform infrared spectra (FTIR) were recorded on a Bruker Vertex 70 ATR-FTIR spectrometer with the RAMII Raman module, equipped with a 1064 nm laser source. Scanning electron microscope (SEM) images were recorded with a Philips XL30 FEG. Before analysis, the samples were coated with 5 nm of Pt. Inductively Coupled Plasma-Optical Emission Spectrometry (ICP-OES) was performed on a Perkin Elmer optical emission spectrometry Optima 8300 instrument. N_2 physisorption isotherm was measured on a Micromeritics 3Flex Surface Analyzer at 77 K. Prior to analysis, the sample was degassed for 12 h under vacuum at 100 ℃.

Computational details

Density functional theory (DFT) calculations were carried out with the Amsterdam Density Functional program (ADF2016).[26] Numerical integration was performed using Becke grid integration.[27] Geometry optimization was conducted using GGA Becke exchange[28] plus the Perdew 86 correlation[29] (BP) functional and all-electron Slater basis sets of triple-ζ quality with one polarization function (TZP).[30] Scalar relativistic effects were accounted for using the Zeroth-Order Regular Approximation (ZORA).[31] Solvation effects were introduced using the COnductor-like Screening MOdel (COSMO) with the default parameters for water (ε = 78.39; solvent radius = 1.93 Å) where solvent-excluding surface (SES) correction was included.[32] Next to geometry optimizations at BP86/TZP/ZORA-Scalar/COSMO, single-point calculations using the hybrid B3LYP functional[29] were performed to calculate different molecular properties (bonding energies, frontier molecular orbitals and molecular electrostatic potentials) of the different binding modes.

RESULTS AND DISCUSSION

Hydrolysis of Gly-Gly

Gly-Gly was chosen as a model dipeptide as its hydrolysis can be easily followed by means of ^{1}H NMR spectroscopy. A mixture containing 2.0 μmol of Gly-Gly and 2.0 μmol of MOF-808 was reacted at 60 °C and pD 7.4. After different time increments the fractions of both the dipeptide and hydrolyzed product were determined (Figure 2). Similar to the reaction in the presence of Zr-POMs[13a, 13c] the by-product, cyclic Gly-Gly (cGly-Gly), formed by the intramolecular condensation between the carboxylate and the amino group was observed during the course of the hydrolytic reaction (Scheme 1). In the absence of MOF-808, neither Gly nor cGly-Gly were observed after 7 months at pD 7.4 and 60 °C. This indicates that MOF-808 catalyzed both the hydrolysis and cyclization processes. Some other artificial metallopeptidases based on Ce(IV) and Zr(IV) have been previously reported to promote the formation of cyclic dipeptide products which were not directly hydrolyzed into individual amino acids.[5, 13a, 13c] Figure 3 shows the percentage of Gly-Gly, cGly-Gly, and Gly as a function of reaction time. The data show that the fraction of cGly-Gly reached a maximum of approximately 10 % after 0.5 h reaction and then gradually decreased. An observed rate constant of 2.69×10^{-4} s^{-1}($t_{½}$ = 0.72 h) for the hydrolysis of Gly-Gly at 60 °C and pD 7.4 was obtained (Figure 4). Table S1 summarizes the observed rate constants for the hydrolysis of Gly-Gly by several Zr(IV)-POMs (Figure S1), as reported in our previous studies.[13a, 13c, 13e] These studies revealed that Zr(IV)-POM based catalysts exhibit only a single active Zr(IV) center that can facilitate the peptide bond hydrolysis. Remarkably, Gly-Gly hydrolysis in the presence of MOF-808 was enhanced by nearly three orders of magnitude compared to the reactions catalyzed by Zr(IV)-POMs under the same experimental conditions. Moreover, a rate constant of 7.4×10^{-9} s^{-1}, corresponding to a half-life of 3 years, was estimated for the uncatalyzed hydrolysis of Gly-Gly at pD 7.2 and 60 °C.[2] This indicates a rate enhancement of 3.6×10^4 times when MOF-808 was used. In addition, in the presence of 10-fold excess of Gly-Gly (20.0 μmol) in comparison to MOF-808 (2.0 μmol) a complete hydrolysis of the peptide bond was obtained with a rate constant of 4.83×10^{-5} s^{-1} ($t_{½}$ = 3.98 h), indicating that the reaction is truly catalytic. To test the heterogeneity, the reaction was stopped after 2 h; MOF-808 was removed via centrifugation and the homogeneous solution was allowed to react further. The percentage of Gly-Gly hydrolyzed before and after the removal of the catalyst is presented in Figure 5. As can be seen, after removing MOF-808 from the reaction mixture, no additional Gly-Gly hydrolysis was observed. This indicates that the outstanding catalytic activity of MOF-808 towards peptide bond hydrolysis is exclusively associated with catalytically active sites of the solid MOF-808. Importantly, MOF-808 could be recycled and reused for the hydrolysis of Gly-Gly for five runs by using ethanol or methanol for washing and exchanging water before the activation process (Figure S2). The reactivity of the individual $Zr_6O_4(OH)_4$ cluster core towards peptide bond hydrolysis was also tested. Benzoate- and methacrylate-capped Zr_6 clusters were synthesized and used to study the cleavage of Gly-Gly under identical experimental conditions as for MOF-808.[25] However, no hydrolysis of Gly-Gly was observed after 5 h, likely due to the coordinatively saturated environment around each Zr(IV) center. The hydrolysis of 2.0 μmol of Gly-Gly by 2.0 μmol of $ZrCl_4$ at pD 7.4 and 60 °C was also studied. A much slower hydrolysis was obtained with an observed rate constant of 5.55×10^{-7} s^{-1}, which corresponds to a half-life of 14.4 days.

The hydrolysis of 2.0 mM Gly-Gly was further studied in the presence of different amounts of MOF-808 ranging from 0.5 μmol to 10.0 μmol. The observed rate constants for the hydrolysis of Gly-Gly were plotted as a function of concentration of MOF-808 (i.e. concertation of $\{Zr_6O_8\}$ clusters) and fitted to a pseudo-Michaelis-Menten model (equation [1]) as shown in Figure 6. [33]

$$k_{obs} = \frac{k_{max} * [MOF-808]}{K_M + [MOF-808]} \qquad [1]$$

where k_{obs} is the observed first-order reaction rate constant, k_{max} is the maximal observed rate constant and K_M is the Michaelis constant which represents the concentration of MOF-808 for which k_{obs} equals $k_{max}/2$. A maximal rate constant k_{max} of 11.0×10^{-4} s^{-1} ($t_{½}$ = 10.5 min) and a Michaelis

constant K_M of 5.42 mM were calculated for the hydrolysis of Gly-Gly by MOF-808 at pD 7.4 and 60 °C.

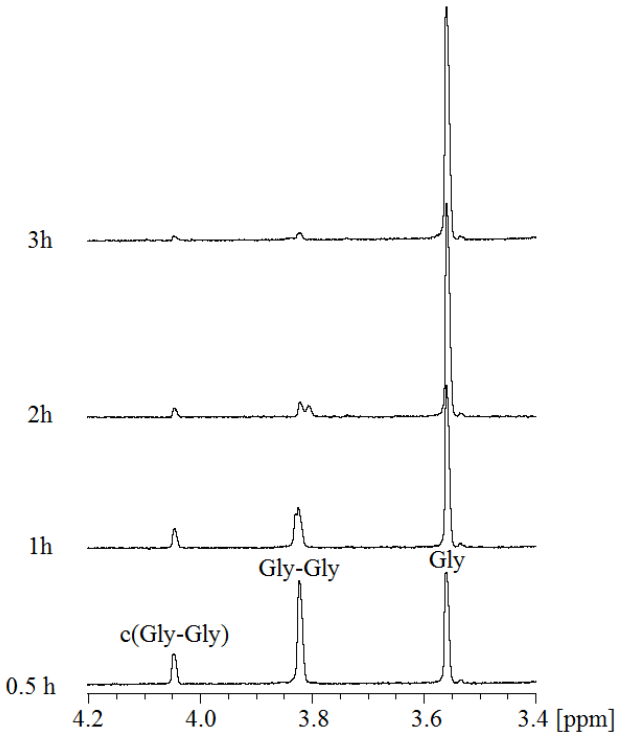

Figure 2. ^{1}H NMR spectra recorded at different reaction times during the hydrolysis of 2.0 μmol of Gly-Gly by 2.0 μmol of MOF-808 at pD 7.4 and 60 °C.

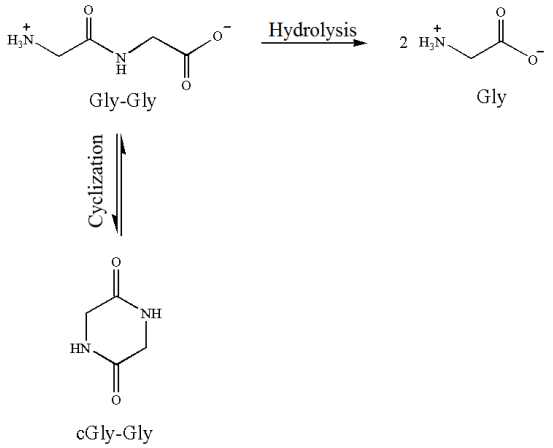

Scheme 1. Hydrolysis of Gly-Gly and its cyclization to cGly-Gly by MOF-808.

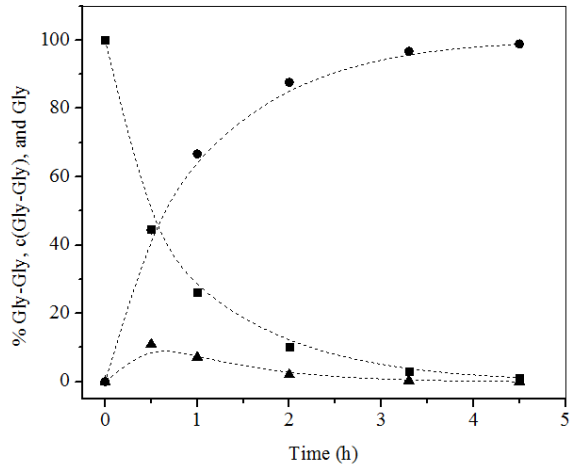

Figure 3. Percentage of Gly-Gly (■), c(Gly-Gly) (▲), and Gly (●) as a function of reaction time for the hydrolysis of 2.0 μmol of Gly-Gly by 2.0 μmol of MOF-808 at pD 7.4 and 60 °C.

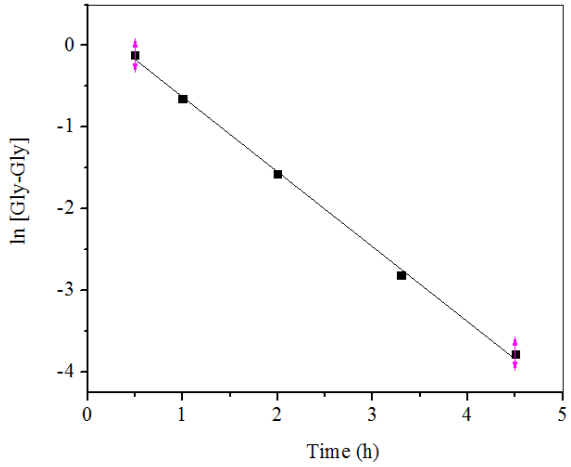

Figure 4. ln[Gly-Gly] as a function of time for the reaction between 2.0 μmol of Gly-Gly and 2.0 μmol of MOF-808 at pD 7.4 and 60 °C.

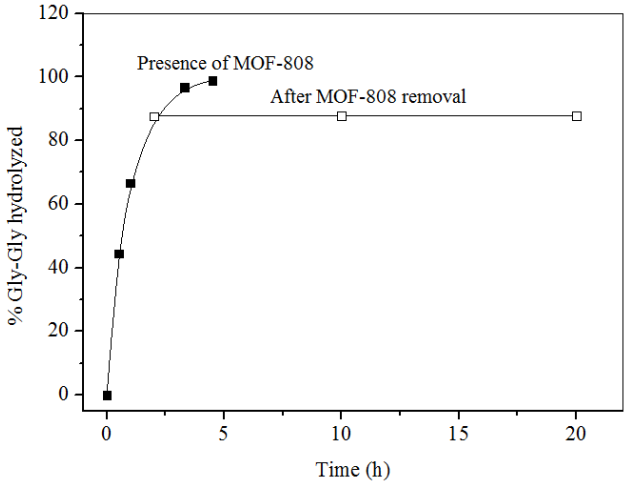

Figure 5. Hydrolysis of 2.0 μmol of Gly-Gly in the presence of 2.0 μmol of MOF-808 (■) before and (□) after the removal of MOF-808 (pD 7.4 and 60 °C).

The effect of pD on Gly-Gly hydrolysis in the presence of MOF-808 was investigated in the pD range from 4.6 to 9.8 at 60 °C. The conversion of Gly-Gly after 4 h in the reaction mixtures containing 2.0 μmol of Gly-Gly and 2.0 μmol of MOF-808 at different pD values is presented in Figure S3. As can be seen from this figure, the reaction was fast over a wide pD range with the fastest reaction occurring under physiological pH. In addition, a slight decrease in the reaction rate at higher pD value was observed. In order to check the effect of pD on the stability of MOF-808 structure, PXRD of the MOF-808 samples after the reaction were recorded (Figure S4). The changes in PXRD that were observed from pD 8.4 onwards could be a result of partial instability of MOF-808 in alkaline conditions, resulting in a slight decrease in catalytic activity.[34] At all lower pH values, the PXRD patterns give no evidence for any structure degradation.

The effect of temperature on the hydrolytic activity of MOF-808 at pD 7.4 was investigated as well. Increasing the reaction temperature from 37 °C to 80 °C resulted in a 25-fold increase of the reaction rate constant and a decrease of the half-life from 4.4 h to 0.17 h. When the data in Figure S5 were fitted to the Arrhenius equation, an experimental activation energy parameter (E_a) of 69 ± 1 kJ mol^{-1} was obtained (Figure S6). This value is significantly higher than what would be expected if the reaction kinetics were determined by a slow diffusion of the dipeptide reactant through the MOF-808 micropores. Comparison of the activation energy of the reaction in the presence of the MOF to the non-catalyzed reaction is difficult due to the extremely slow rate of the latter. However, one can compare with the E_a values that were previously determined for Gly-Gly hydrolysis in the presence of Zr(IV)-Keggin and Wells-Dawson POMs, and which were in the range of 90 - 91 kJ mol^{-1}.[13a, 13c] This indicates that in the presence of MOF-808 the activation energy for the hydrolysis of Gly-Gly is lowered by ca. 22 kJ mol^{-1}. Linear fitting of ln(k_{obs}/T) as a function of 1/T (Figure S7) allows for the calculation of the enthalpy of activation, $\Delta H^{\#}$ = 66 ± 1 kJ mol^{-1}, and entropy of activation, $\Delta S^{\#}$ = –116 ± 1 J mol^{-1} K^{-1}. The Gibbs energy of activation ($\Delta G^{\#}$) for the hydrolysis of Gly-Gly at 37 °C is 105 ± 1 kJ mol^{-1}. The negative activation entropy obtained is most likely the result of the coordination of the dipeptides to the Zr sites.

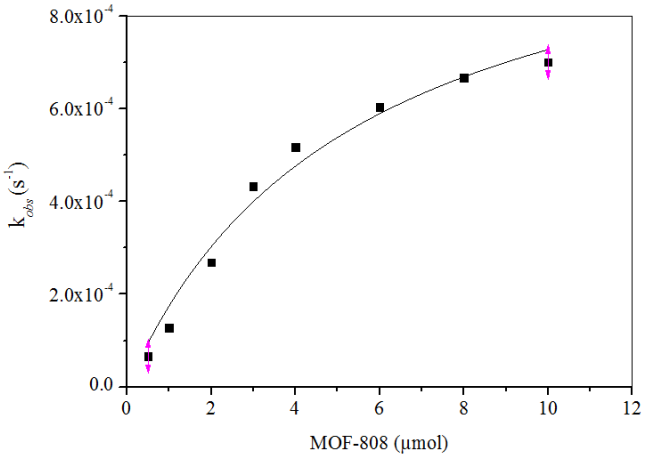

Figure 6. Influence of the amounts of MOF-808 on the rate constant for the hydrolysis of 2.0 mM Gly-Gly at pD 7.4 and 60 °C.

Analysis of the Gly-Gly adsorption in MOF-808

The sizes of the primary cages of MOF-808 (ca. 18 Å)[35] are sufficiently large to accommodate dipeptide species. In order to gain insight into the ability of MOF-808 to capture peptides, the adsorption of Gly-Gly on MOF-808 was studied at pD 7.4 and room temperature. To avoid the hydrolysis of Gly-Gly by MOF-808, the adsorption was studied within 30 min at room temperature. The adsorption of 2.0 μmol of Gly-Gly on 2.0 μmol of MOF-808 as a function of time is shown in Figure S8. The result shows that Gly-Gly was quickly adsorbed and the adsorption of Gly-Gly was at equilibrium after 10 min stirring at room temperature. In order to study the capacity of MOF-808 for Gly-Gly adsorption, mixtures containing 2.0 μmol of MOF-808 and 0.5-50.0 μmol of Gly-Gly were stirred for 30 min at pD 7.4 and room temperature. As can be seen in Figure S9, the amount of Gly-Gly adsorbed on the solid phase of MOF-808 increased with an increase of the initial concentration of Gly-Gly. A saturation adsorption capacity of 1.15 mmol of Gly-Gly per g of MOF-808 (0.65 mmol of Zr_6O_8 cluster) was obtained.

Hydrolysis of Gly-Gly-NH_2 and Gly-Gly-Ala

In order to get more insight in the binding mode of Gly-Gly to MOF-808, the hydrolysis of 2.0 μmol of Gly-Gly-Ala and Gly-Gly-NH_2 in the presence of 2.0 μmol of MOF-808 was investigated at pD 7.4 and 60 °C. An overview of the chemical structures of these substrates is presented in Table 1.

As can be seen from the ^{1}H NMR spectra of Gly-Gly-Ala hydrolyzed by MOF-808 (Figure S10), after 5 minutes at 60 °C Gly (3.56 ppm), Ala (1.45–1.47 ppm), and Gly-Ala (1.35–1.37 ppm) were all observed. The immediate formation of these products indicates that the hydrolysis of the N-terminal peptide bond occurred simultaneously with the hydrolysis of the C-terminal peptide bond in this tripeptide. After 30 minutes of reaction, the signals of the methyl group of Ala-Gly at 1.53–1.55 ppm were clearly seen. The formation of Ala-Gly is a result of ring-opening of c(Gly-Ala) which is the cyclisation product of Gly-Ala (Figure s11) formed from Gly-Ala, obtained during the

hydrolysis of Gly-Gly-Ala.[13g] The percentage of the hydrolyzed product Gly as a function of time is presented in Figure S12. A rate constant k_{obs} of 2.06×10^{-4} s^{-1} ($t_{1/2}$ = 0.93 h) was obtained for the formation of Gly. However, the rate constant of Ala formation cannot be calculated from the NMR spectra due to the overlap of the methyl group in Ala and c(Gly-Ala).

The hydrolysis progress of Gly-Gly-NH_2 in the presence of MOF-808 is shown in Figure S13. After 5 minutes of reaction, Gly was still below the limit of detection. Since the signals of Gly-Gly and Gly-NH_2 are overlapped, it is impossible to identify which bond was preferentially cleaved. However, a rate constant for the formation of Gly out of this peptide (k_{obs}= 0.55×10^{-4} s^{-1}, corresponding to a half-life of 3.5 h) could be calculated. This shows that the conversion of Gly-Gly-NH_2 to Gly is more than three times slower than that of Gly-Gly-Ala. Obviously, when the peptides are blocked at the C-terminal end the reaction rates are lower than for the unblocked peptides. From these results we can conclude that the terminal carboxylate group is directly involved in the acceleration of the hydrolysis process when MOF-embedded Zr centers are used.

Table 1. Observed rate constants for the formation of Gly from the hydrolysis of Gly-Gly-Ala and Gly-Gly-NH_2 by MOF-808 at pD 7.4 and 60 °C.

Substrate	$10^4 k_{obs}$ (s^{-1})	$t_{1/2}$ (h)
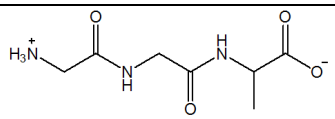 Gly-Gly-Ala	2.06	0.93
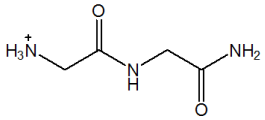 Gly-Gly-NH_2	0.55	3.50

Inhibition studies

Further insight into the coordination of Gly-Gly to MOF-808 was obtained by following the hydrolysis of Gly-Gly by MOF-808 in the presence of several nonreactive carboxylic acids (Figure 7). These inhibitors have multiple carboxylic groups which can coordinate to the oxophilic Zr(IV), thus blocking the access of the substrate.

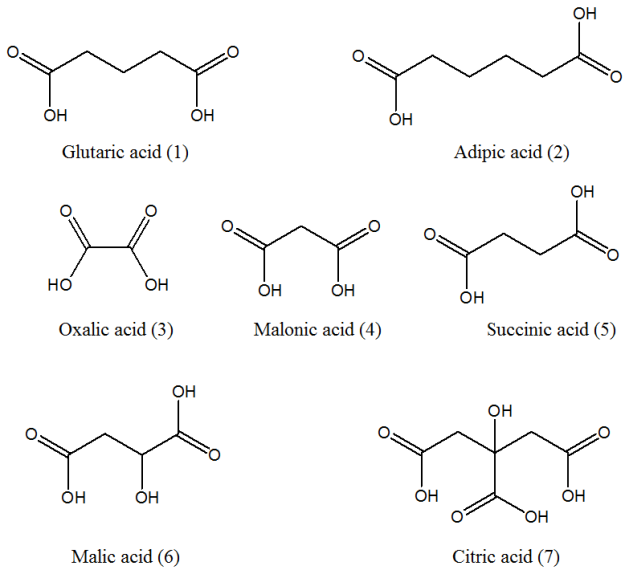

Figure 7. Chemical structures of the examined inhibitors

Figure 8 provides an overview of the conversion of Gly-Gly in the presence of the inhibitors. In all cases the presence of the carboxylic acid inhibitors causes a decrease in the reaction rate for the hydrolysis of Gly-Gly. The strongest inhibition effect (ca. 90 %) was observed in the presence of acids with short aliphatic chain lengths while the dicarboxylic acids with longer aliphatic chains caused a rate decrease of approximately 72 %. These nonreactive carboxylic acids are known to act as multidentate ligands for many metal ions,[36] and therefore, the observed effect of reduced Gly-Gly hydrolysis in the presence of these inhibitors is likely due to a competitive coordination of Zr(IV) to the carboxyl and hydroxyl groups. Notably, the inhibition effect of dicarboxylic acids is ca. two-fold stronger than that of monocarboxylic acids (Figure S14). In addition, the inhibition trends observed here are similar to those in the presence of Zr-POMs indicating that both carboxylate groups of diacids act in chelating with the $\{Zr_6O_8\}$ core.[13b, c, 13e]

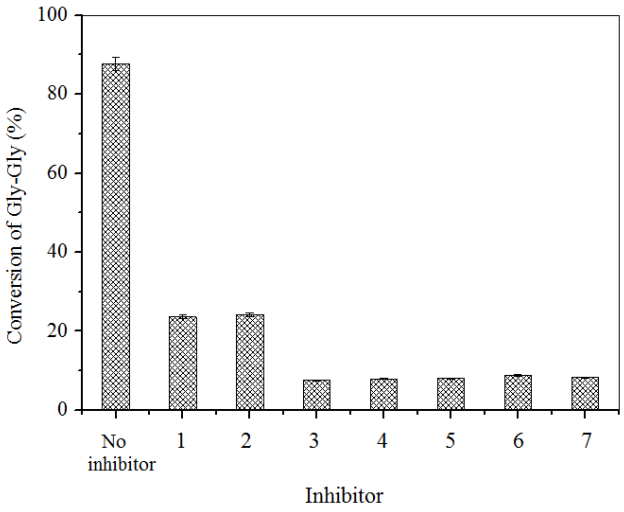

Figure 8. Conversion of Gly-Gly after 2 h in the reactions containing 2.0 μmol of Gly-Gly, 2.0 μmol of MOF-808, and 5.0 μmol of the inhibitor at pD 7.4 and 60 °C.

Hydrolysis of Gly-X dipeptides

The catalytic activity of MOF-808 towards dipeptides containing different X amino acid side chains at the C-terminus was examined at pD 7.4 and 60 °C. Considering the potential intermolecular interactions between the btc linkers and dipeptides and the entrance in the MOF-808 pores, we selected a group of dipeptides that differ in terms of size, hydrophobicity index[37] and additional functionalities. The conversion of the selected dipeptides in presence of MOF-808 over 2 h was plotted as a function of the side chain volume (Figure 9). Our results show that the catalytic hydrolysis of neutral or highly hydrophilic dipeptides is highly dependent on the volume of the amino acid side chains. Thus, their conversion decreased with an increase in the side chain bulkiness: Gly-Gly > Gly-Ala > Gly-Asp > Gly-Asn > Gly-Lys ≈ Gly-Arg. This is a logical outcome as steric hindrance can hinder the access of the amide carbonyl oxygen atom to the active $\{Zr_6O_8\}$ core and can potentially limit the diffusion of the dipeptides in the pores of MOF-808. Gly-X dipeptides with clearly hydrophobic X residues (e.g. Val, Leu, Ile) are less reactive for the hydrolytic conversion than dipeptides with neutral or hydrophilic X residues. Indeed, these residues (group II) lack electron rich functionalities and therefore cannot engage in favourable intermolecular interactions with the btc linkers, while their pronounced hydrophobicity impacts the interaction with the active core and the diffusion into the MOF-808 pores. On the other hand, reaction rates are higher than expected for Met and Phe (group I): their hydrophobic residues contain electron rich thiol and aromatic functionalities which can facilitate intermolecular thiol-aromatic bonding[38] or π-π stacking respectively.

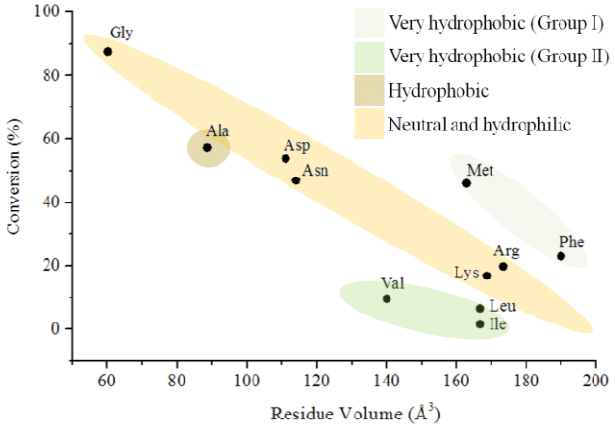

Figure 9. Conversion after 2 h at pD 7.4 and 60 °C for the hydrolysis of 2.0 μmol of Gly-X dipeptides in the presence of 2.0 μmol of MOF-808 as a function of the volume of amino acid X.

Stability of MOF-808

Figure S17a represents the N_2 physisorption isotherm for the MOF-808 material used in our experiments. The isotherm features two distinct steps in N_2 uptake, representing adsorption in the different cages of MOF-808. As shown by the calculated pore size distribution (Figure 17b), indeed both the small tetrahedral cage of ~7-10 Å in size and the much larger adamantine-type cage (18.4 Å) are resolved. Using the BET method, a specific surface area of 1820 m^2/g was calculated. The t-plot calculation revealed a micropore area of 1333 m^2/g and an external surface area of 487 m^2/g.

The stability of MOF-808 under the experimental conditions was examined by several complementary techniques including ^{1}H NMR spectroscopy, ICP, FT-IR, PXRD, and SEM for the samples before and after the catalytic process. The abortion of the Gly-Gly hydrolysis directly after the removal of MOF-808 was the first indication that MOF-808 is not leaching Zr(IV) ions or $\{Zr_6O_8\}$ cores, which could also facilitate the peptide hydrolysis, into solution. In order to confirm this, the reaction mixture containing 2.0 μmol of Gly-Gly and 2.0 μmol of MOF-808 at pD 7.4 was centrifuged after 2 h reaction at 60 °C to remove MOF-808. The solution after catalyst removal was used to measure ICP. The result shows that Zr(IV) was below the detection limit (20 ppb). In addition, ^{1}H NMR spectra of the acid digested MOFs show that negligible linker had leached from the framework after the reaction. Moreover, FT-IR spectra and PXRD patterns of MOF-808 before and after reaction were recorded and are shown in Figure S15 and Figure S16. The resemblance of FT-IR spectra and PXRD patterns before and after the reaction further corroborates the stability of MOF-808 under the experimental conditions, even after the second reaction cycle. Moreover, from SEM images of MOF-808 taken before and after reactions (Figure S17c), it is evident that the MOF-808 crystals retain their octahedral morphology, demonstrating that the bulk MOF-808 exhibits a remarkable stability over the catalytic process.

The effect of organic solvents on the process of washing MOF-808 after use was studied. Direct activation of MOF-808 after washing with water compromises the MOF structure due to the high surface tension of water, yielding a poor activity.[39] Therefore, several organic solvents were used to wash and exchange water before activation at high temperature to avoid damage to the MOF structure. As can be seen in Figure 10, the Gly-Gly hydrolysis activity for the second reaction cycle was recovered when acetonitrile, methanol or ethanol were used before the activation process. PXRD indicated that MOF-808 treated with methanol after the second reaction cycle remained unchanged (Figure S16).

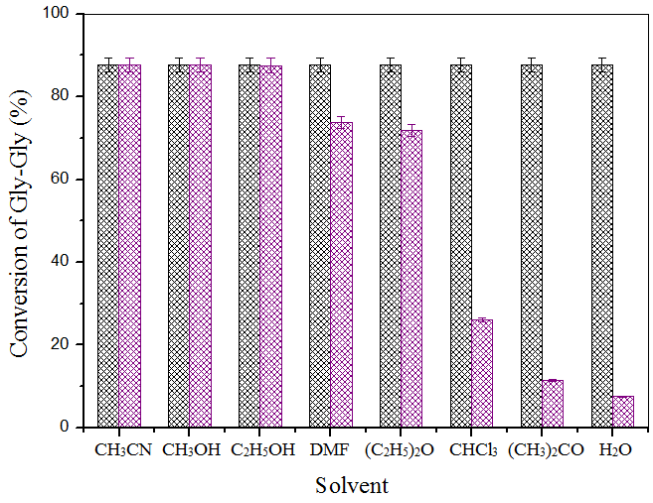

Figure 10. Conversion of Gly-Gly after 2 h at 60 °C for the first (black) and second (purple) reaction cycles. Different organic solvents were used to wash and exchange water before activation at 150 °C.

Atomistic insights into the Gly-Gly dipeptide bond activation

In order to design a suitable model that can provide atomistic insights into the dipeptide bond activation, we take into account two experimental observations: *i*) MOF-808 exhibits remarkable stability during the catalytic process; *ii*) the catalytic efficiency is dependent on the residue-linker interactions. These two observations, including the recent theoretical studies on MOF-808 cores by Morris and coworkers,[40] support our belief that the $\{Zr_6O_8\}$ core solely provides catalytic sites while the btc-peptide residue interactions fine-tune the process efficiency. Following this, the loss of a carboxylate bearing moiety, most likely formate, exposes a pair of electrophilic Zr(IV) centres that defines the catalytically active site for the peptide hydrolysis process.

The small Gly-Gly molecules can interact directly with the $\{Zr_6O_8\}$ cores without developing significant linker-substrate interactions that affect the interaction geometry. This provides us with an advantage to virtually replace all btc ligands by single formate ligands and thus to focus solely on the changes of the electronic structure as a function of the interaction geometry. The influence of protonation of the $\{Zr_6O_8\}$ cores was evaluated by considering non-protonated and tetraprotonated $\{Zr_6O_4(OH)_4\}$ores.

Geometry optimizations of our first model $[Zr_6O_8(HCOO)_{12}]^{4-}$ at BP86 level provided a good approximation of the relevant bond lengths (Zr–O and C–C) and interatomic (Zr···Zr) distances especially when compared to those experimentally obtained for MOF-808 (Table S2). Single point calculation of the $[Zr_6O_8(HCOO)_{12}]^{4-}$ model at B3LYP level shows a high energy gap (ca. 5.7 eV) between the highest occupied molecular orbital (HOMO) and the lowest unoccupied molecular orbital (LUMO) (Figure 11). This is an expected feature for fully-oxidized Zr(IV) based materials that exhibit an O-dominated HOMO and a Zr-dominated LUMO (*d*-atomic like orbitals) resembling the oxo and metal band respectively typical for extended solids.[41]

The replacement of the single formate ligand with single deprotonated Gly-Gly$^-$ (= $NH_2CH_2CONHCH_2COO^-$) leads to a $[Zr_6O_8(HCOO)_{11}(Gly\text{-}Gly)]^{4-}$ model core. We have investigated three different binding mode configurations: a) *mode 1* featuring Gly-Gly$^-$ binding via the two O atoms of the terminal carboxylate ligand; b) *mode 2* featuring Gly-Gly$^-$ interaction with the $\{Zr_6O_8\}$ core via two O atoms deriving from the carboxylate and from the amide functionality; c) *mode 3* featuring binding via O atom from the amide group and N atom of the N-terminus. Relative to mode 3, mode 1 and mode 2 lay 55.3 kJ·mol^{-1} and 5.5 kJ·mol^{-1} higher in bonding energy respectively (Table S3). The small difference in relative bonding energy especially between modes 2 and 3 suggests that the binding modes have similar stability and therefore they are in a close competition with each other. The energy and the character of the HOMO in binding modes 1, 2 and 3 is similar and comparable to that of $[Zr_6O_8(HCOO)_{12}]^{4-}$, which suggests that the Gly-Gly does not alter the electronic structure of the $\{Zr_6O_8\}$ core (Figure 11). However, depending on the binding mode, the character and the energy of the LUMO are severely altered. In the case of mode 1 where the binding of Gly-Gly occurs via the carboxylate moiety, the LUMO is virtually similar to that of $[Zr_6O_8(HCOO)_{12}]^{4-}$. In binding mode 2, the LUMO is predominantly distributed over the Zr-centers, while minor electron distribution occurs over the N and C centers of the bound Gly-Gly moiety. Finally, mode 3 features a LUMO predominantly distributed over the C and N atoms of the peptide bond depicting *p*-atomic like orbitals arranged in an antibonding fashion along the peptide bond. Population of this orbital will consequently destabilize the dipeptide bond. Further, the LUMO in mode 3 is lower in energy than the LUMOs in mode 1 and mode 2. This implies that upon binding in mode 3, the unoccupied antibonding orbital coming from the Gly-Gly molecules is effectively lowered.

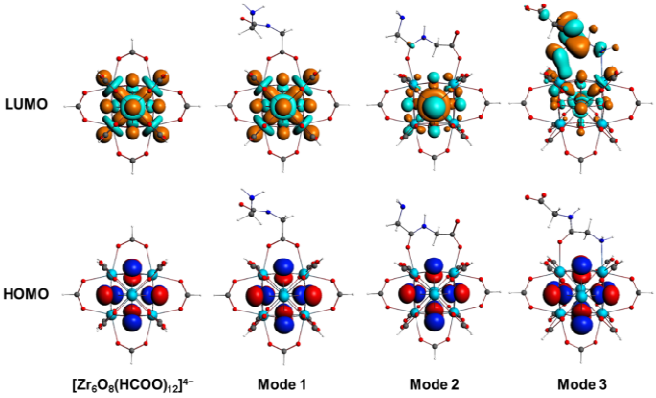

Figure 11. Frontier molecular orbitals HOMO (bottom row) and LUMO (top row) plotted over ball-and-stick representations of the $[Zr_6O_8(HCOO)_{12}]^{4-}$ cluster and the three binding modes of $[Zr_6O_8(HCOO)_{11}(gly\text{-}gly)]^{4-}$ model systems. Colour code: Zr = light blue, O = red, C = black and H = white.

Decoration of $[Zr_6O_8(HCOO)_{12}]^{4-}$ with four protons arranged in a tetrahedral fashion around the O atoms of $\{Zr_6O_8\}$ leads to a $[Zr_6(OH)_4O_4(HCOO)_{12}]$ model that can be subject to further formate ligand replacement with Gly-Gly$^-$ ligands. Considering the three binding modes (mode 1-3) of $[Zr_6O_8(HCOO)_{11}(Gly\text{-}Gly)]^{4-}$, six analogous neutral isomers can respectively be constructed for $[Zr_6(OH)_4O_4(HCOO)_{11}(Gly\text{-}Gly)]$ which differ with respect to the relative disposition of the dipeptide moiety to the four protons of the $\{Zr_6O_8\}$ core (Figure S18). Our optimizations and single point calculations have shown that the six binding modes are differing within 26 kJ·mol^{-1} (Table S4). As the four protons bind directly to the $\{Zr_6O_8\}$ core, all of the six modes of $[Zr_6(OH)_4O_4(HCOO)_{11}(Gly\text{-}Gly)]$ exhibit Zr-based LUMO's. The unoccupied MOs that exhibit antibonding interactions along the peptide bond appear lowest in energy in 3a and 3b and respectively lay at -1.8 eV and -1.5 eV on the energy scale. (Figure S19). Unoccupied MOs with antibonding character are also present in the isomeric modes 1a and 1b; however they lay above -0.5 eV on the energy scale. This shows that even under a tetraprotonated scenario (i.e. having $\{Zr_6O_4(OH)_4\}$ cores), Gly-Gly binding to the two Zr(IV) centers via the oxygen atom from the amide group at the N-terminus remains the most attractive coordination mode that can facilitate the peptide bond activation and hydrolysis.

The above discussed calculations show that the degree of protonation does not affect the relative stability order between the different binding modes, however it does affects the energy difference in each individual model set. In this context it can be very difficult to accurately calculate and predict a reaction mechanism for the hydrolysis of dipeptides and polypeptides by MOF 808. However, the preservation of the bonding energy trends and the calculated relative bonding energy ranges for both protonated and unprotonated scenarios, hint that in aqueous media different modes of Gly-Gly are competing with one another to access the catalytic site of $\{Zr_6O_8\}$ cores. Such competition is only further augmented in the presence of inhibitors (*vide supra*). From the different bonding modes, only mode 3 can successfully promote the peptide bond activation and hydrolysis, while similar relevance of this type of binding mode has been outlined in our recent work focusing on the interaction and hydrolysis of dipeptides with Zr(IV) substituted Keggin polyanions.[14]

Hydrolysis of Hen Egg White Lysozyme (HEWL) by MOF-808

The reactivity of MOF-808 was further tested on HEWL, a 14.3 kDa protein containing 129 amino acids. HEWL was incubated with MOF-808 at 60 °C and subsequently reaction aliquots were taken at different time intervals and analyzed by SDS-PAGE to evaluate the progressive hydrolysis of HEWL in the presence of MOF-808. Figure 12 shows the SDS-PAGE image of HEWL hydrolysis. The appearance of new bands with lower molecular weights during the course of the reaction indicates that selective HEWL hydrolysis occurred. As can be seen in Figure 12 and Figure S20, the hydrolysis of HEWL in the presence of MOF-808 already occurred after 1 h incubation. After 25 h reaction ca. 55% HEWL was hydrolyzed (Table S5), resulting in fragment bands with molecular weights (MWs) of approximately 12.2, 10.7, 8.2, and 6.4 kDa. The MWs of the fragments suggest that the HEWL was most likely selectively hydrolyzed at 3 peptide bonds. The fragments at 8.2 and 6.4 kDa are likely originating from one cleavage site as their added MW is close to the MW of the intact HEWL. The shorter fragments that result from the cleavage at the second and the third site (that produced larger fragment at 12.2 and 10.7 kDa) unfortunately could not be observed as short polypeptides tend to leak from the SDS PAGE gel. The cleavage of HEWL under physiological pH and temperature was also tested (Figure S21). At 37 °C the bands appeared at the same position in SDS-PAGE gel as observed at 60 °C, indicating the presence of the fragments having the same molecular weight. The control experiments showed that hydrolysis of HEWL was not observed in the absence of MOF-808 at 37 °C or even at 60 °C (Figure S21 and Figure S22), confirming the catalytic role of MOF-808 in protein hydrolysis. Analysis of the cleavage sites and the mechanism of HEWL hydrolysis by MOF-808 are currently underway. Nevertheless, these results already demonstrate the unprecedented ability of MOF-808 to catalyze hydrolysis of extremely stable peptide bonds in proteins. Two possible hypotheses can be put forward for the interaction between the HEWL protein and MOF-808. While in theory HEWL is too large (3.5 x 2.5 x 4.5 nm^3) to diffuse through the pore windows of MOF-808 (18.4 Å) to access the clusters located in the interior of the framework, previous work by Chen et al. has shown that partial unfolding of the protein structure can enable diffusion into the pores of a MOF, as exemplified by the uptake of Cyt c in Tb-mesoMOF.[42] Alternatively, an initial hydrolysis step can occur on the outer surface of the octahedral MOF-808 crystals, which are terminated with (111) facets. While the exact surface termination of MOF-808 is not known at present, the (111) lattice plane cuts halfway through the large pores of the MOF-808 framework, which likely results in half-spherical pockets on the surface of the crystals. These are of similar size as the smallest dimension of the HEWL protein (~1.8 nm vs ~2.5 nm) and could provide several interaction sites between Zr-nodes and the protein (Figure s23). For the crystals of MOF-808 prepared in this manuscript, approximately 1% of the clusters are exposed on the surface. Once an initial cleavage has occurred, it is possible that these fragments diffuse into the crystal to undergo further hydrolysis.

Direct comparison between these results and the previously reported hydrolysis of bovine serum album (BSA) by HKUST-1 (or [Cu3(btc)2] (btc = benzene-1,3,5-tricarboxylate))[21] is not straightforward due to different structures of these MOFs and different reaction conditions and protein substrates used in these studies. However, in order to observe efficient BSA hydrolysis, alkaline pH conditions of up to pH = 9 were needed in the previous study. This also resulted in leaching of Cu(II) from

the framework, suggesting limited stability of HKUST-1 under the conditions used for BSA hydrolysis.

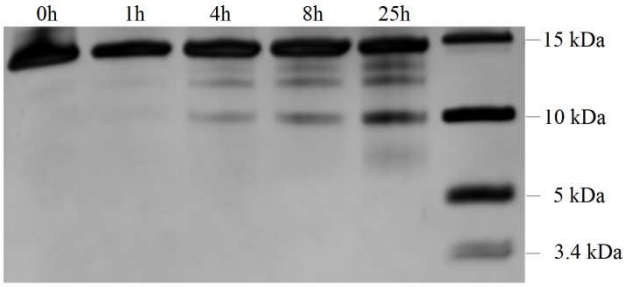

Figure 12. Silver stained SDS-PAGE gel of HEWL hydrolysis in the presence of MOF-808 at 60 °C.

CONCLUSION

A Zr(IV)-containing metal-organic framework, MOF-808, was shown to be highly active towards the hydrolysis of dipeptides under conditions that are pertinent to physiological pH and temperature. The results revealed that MOF-808 is a truly heterogeneous and reusable catalyst, with an activity towards the peptide bond that is far superior compared to other reported Zr(IV)-containing salts or complexes. The combination between experimental studies and calculations revealed that the activity of MOF-808 towards Gly-Gly hydrolysis is due to the ability to form active complexes with two adjacent Zr(IV) centers of the $\{Zr_6O_8\}$ core via the amide oxygen and the amine nitrogen atoms. The catalytic reactivity of MOF-808 towards dipeptides is dependent on the bulkiness and nature of side chain amino acids. Dipeptides with smaller or hydrophilic residues are preferentially hydrolyzed over those with bulky and hydrophobic residues. Interestingly, MOF-808 also promotes selective hydrolysis of HEWL protein under physiological pH. To the best of our knowledge, this is the first example of peptide bond hydrolysis catalyzed by a stable metal-organic framework which provides new and growing opportunities for metal-organic frameworks as a novel class of artificial proteases.

ASSOCIATED CONTENT

Supporting Information

Supporting Information Available: Kinetic data for the hydrolysis of peptides by MOF 808, SDS-PAGE gel and 3D image of HEWL hydrolysis by MOF 808, PXRD, FT-IR and SEM characterization of MOF 808, and detailed results of DFT calculations are provided as Supporting information. This material is available free of charge via the internet at http://pubs.acs.org.

AUTHOR INFORMATION

Corresponding Authors

*tatjana.vogt@kuleuven.be

*dirk.devos@kuleuven.be

ACKNOWLEDGEMENT

H.G.T.L. and B. B thank the FWO (Research Foundation – Flanders) for the postdoctoral fellowship. T.N.P.V. thanks KU Leuven for the financial support under project OT/13/060. T.N.P.V and D.D.V. thank FWO for the financial support under project G095017N. A.K. thanks FWO for the postdoctoral fellowship and the Excellence Initiative of the German Federal Ministry of Education and Research (StUpPD_270-17). G. F. thanks the CSC for fellowships.

REFERENCES

1. (a) Grant, K. B.; Kassai, M. *Curr. Org. Chem.* **2006,** *10*, 1035-1049; (b) Wu, J. H.; Perrin, D. M.; Sigman, D. S.; Kaback, H. R. *Proc. Nat. Acad. Sci. USA* **1995,** *92*, 9186-9190; (c) Zaychikov, E.; Martin, E.; Denissova, L.; Kozlov, M.; Markovtsov, V.; Kashlev, M.; Heumann, H.; Nikiforov, V.; Goldfarb, A.; Mustaev, A. *Science* **1996,** *273*, 107-109; (d) Montigny, C.; Jaxel, C.; Shainskaya, A.; Vinh, J.; Labas, V.; Moller, J. V.; Karlish, S. J. D.; le Maire, M. *J. Biol. Chem.* **2004,** *279*, 43971-43981; (e) Wezynfeld, N. E.; Frączyk, T.; Bal, W. *Coord. Chem. Rev.* **2016,** *327–328*, 166-187.

2. Radzicka, A.; Wolfenden, R. *J. Am. Chem. Soc.* **1996,** *118*, 6105-6109.

3. Yashiro, M.; Sonobe, Y.; Yamamura, A.; Takarada, T.; Komiyama, M.; Fujii, Y. *Org. Biomol. Chem.* **2003,** *1*, 629-632.

4. (a) Kassai, M.; Ravi, R. G.; Shealy, S. J.; Grant, K. B. *Inorg. Chem.* **2004,** *43*, 6130-6132; (b) Kassai, M.; Grant, K. B. *Inorg. Chem. Commun.* **2008,** *11*, 521-525.

5. Takarada, T.; Yashiro, M.; Komiyama, M. *Chem. Eur. J.* **2000,** *6*, 3906-3913.

6. Rhee, M.-J.; Storm, C. B. *J. Inorg. Biochem.* **1979,** *11*, 17-24.

7. (a) Fujii, Y.; Kiss, T.; Gajda, T.; Tan, X. S.; Sato, T.; Nakano, Y.; Hayashi, Y.; Yashiro, M. *J. Biol. Inorg. Chem.* **2002,** *7*, 843-851; (b) Suh, J. *Acc. Chem. Res.* **2003,** *36*, 562-570; (c) de Oliveira, M. C. B.; Scarpellini, M.; Neves, A.; Terenzi, H.; Bortoluzzi, A. J.; Szpoganics, B.; Greatti, A.; Mangrich, A. S.; de Souza, E. M.; Fernandez, P. M.; Soares, M. R. *Inorg. Chem.* **2005,** *44*, 921-929.

8. Bordignon Luiz, M. T.; Szpoganicz, B.; Rizzoto, M.; Basallote, M. G.; Martell, A. E. *Inorg. Chim. Acta* **1999,** *287*, 134-141.

9. (a) Milović, N. M.; Kostić, N. M. *J. Am. Chem. Soc.* **2002,** *124*, 4759-4769; (b) Parac, T. N.; Kostic, N. M. *J. Am. Chem. Soc.* **1996,** *118*, 5946-5951; (c) Zhu, L. G.; Qin, L.; Parac, T. N.; Kostic, N. M. *J. Am. Chem. Soc.* **1994,** *116*, 5218-5224; (d) Milinkovic, S. U.; Parac, T. N.; Djuran, M. I.; Kostic, N. M. *J. Chem. Soc., Dalton Trans.* **1997**, 2771-2776.

10. (a) Krezel, A.; Mylonas, M.; Kopera, E.; Bal, W. *Acta Biochim. Pol.* **2006,** *53*, 721-727; (b) Protas, A. M.; Bonna, A.; Kopera, E.; Bal, W. *J. Inorg. Biochem.* **2011,** *105*, 10-16; (c) Kopera, E.; Krezel, A.; Protas, A. M.; Belczyk, A.; Bonna, A.; Wyslouch-Cieszynska, A.; Poznanski, J.; Bal, W. *Inorg. Chem.* **2010,** *49*, 6636-6645.
11. Martin, R. B. *Met. Ions Biol. Syst.* **2001,** *38*, 1.
12. (a) Parac, T. N.; Ullmann, G. M.; Kostic, N. M. *J. Am. Chem. Soc.* **1999,** *121*, 3127-3135; (b) Parac, T. N.; Kostic, N. M. *J. Am. Chem. Soc.* **1996,** *118*, 51-58.
13. (a) Absillis, G.; Parac-Vogt, T. N. *Inorg. Chem.* **2012,** *51*, 9902-9910; (b) Ly, H. G. T.; Absillis, G.; Bajpe, S. R.; Martens, J. A.; Parac-Vogt, T. N. *Eur. J. Inorg. Chem.* **2013,** *2013*, 4601-4611; (c) Ly, H. G. T.; Absillis, G.; Parac-Vogt, T. N. *Dalton Trans.* **2013,** *42*, 10929-10938; (d) Ly, H. G. T.; Absillis, G.; Parac-Vogt, T. N. *Eur. J. Inorg. Chem.* **2015,** *2015*, 2206-2215; (e) Ly, H. G. T.; Mihaylov, T.; Absillis, G.; Pierloot, K.; Parac-Vogt, T. N. *Inorg. Chem.* **2015,** *54*, 11477-11492; (f) Ly, H. G. T.; Absillis, G.; Parac-Vogt, T. N. *New J. Chem.* **2016,** *40*, 976-984; (g) Vanhaecht, S.; Absillis, G.; Parac-Vogt, T. N. *Dalton Trans.* **2013,** *42*, 15437-15446; (h) Stroobants, K.; Absillis, G.; Shestakova, P. S.; Willem, R.; Parac-Vogt, T. N. *J. Cluster Sci.* **2014,** *25*, 855-866.
14. Mihaylov, T. T.; Ly, H. G. T.; Pierloot, K.; Parac-Vogt, T. N. *Inorg. Chem.* **2016,** *55*, 9316-9328.
15. (a) Ly, H. G. T.; Absillis, G.; Janssens, R.; Proost, P.; Parac-Vogt, T. N. *Angew. Chem. Int. Ed.* **2015,** *54*, 7391-7394; (b) Stroobants, K.; Moelants, E.; Ly, H. G. T.; Proost, P.; Bartik, K.; Parac-Vogt, T. N. *Chem. Eur. J.* **2013,** *19*, 2848-2858; (c) Stroobants, K.; Absillis, G.; Moelants, E.; Proost, P.; Parac-Vogt, T. N. *Chem. Eur. J.* **2014,** *20*, 3894-3897.
16. (a) Zhou, H. C.; Kitagawa, S. *Chem. Soc. Rev.* **2014,** *43*, 5415-5418; (b) Long, J. R.; Yaghi, O. M. *Chem. Soc. Rev.* **2009,** *38*, 1213-1214.
17. Lu, W. G.; Wei, Z. W.; Gu, Z. Y.; Liu, T. F.; Park, J.; Tian, J.; Zhang, M. W.; Zhang, Q.; Gentle, T.; Bosch, M.; Zhou, H. C. *Chem. Soc. Rev.* **2014,** *43*, 5561-5593.
18. (a) Farrusseng, D.; Aguado, S.; Pinel, C. *Angew. Chem.-Int. Edit.* **2009,** *48*, 7502-7513; (b) Ma, L.; Abney, C.; Lin, W. *Chem. Soc. Rev.* **2009,** *38*, 1248-1256; (c) Kesanli, B.; Lin, W. *Coord. Chem. Rev.* **2003,** *246*, 305-326; (d) Lee, J.; Farha, O. K.; Roberts, J.; Scheidt, K. A.; Nguyen, S. T.; Hupp, J. T. *Chem. Soc. Rev.* **2009,** *38*, 1450-1459.
19. (a) Katz, M. J.; Brown, Z. J.; Colon, Y. J.; Siu, P. W.; Scheidt, K. A.; Snurr, R. Q.; Hupp, J. T.; Farha, O. K. *Chem. Commun.* **2013,** *49*, 9449-9451; (b) Cavka, J. H.; Jakobsen, S.; Olsbye, U.; Guillou, N.; Lamberti, C.; Bordiga, S.; Lillerud, K. P. *J. Am. Chem. Soc.* **2008,** *130*, 13850-13851; (c) Bai, Y.; Dou, Y.; Xie, L.-H.; Rutledge, W.; Li, J.-R.; Zhou, H.-C. *Chem. Soc. Rev.* **2016,** *45*, 2327-2367.
20. (a) Katz, M. J.; Moon, S.-Y.; Mondloch, J. E.; Beyzavi, M. H.; Stephenson, C. J.; Hupp, J. T.; Farha, O. K. *Chem. Sci.* **2015,** *6*, 2286-2291; (b) Moon, S. Y.; Liu, Y. Y.; Hupp, J. T.; Farha, O. K. *Angew. Chem.-Int. Edit.* **2015,** *54*, 6795-6799; (c) Mondloch, J. E.; Katz, M. J.; Isley, W. C., III; Ghosh, P.; Liao, P.; Bury, W.; Wagner, G.; Hall, M. G.; DeCoste, J. B.; Peterson, G. W.; Snurr, R. Q.; Cramer, C. J.; Hupp, J. T.; Farha, O. K. *Nat. Mater.* **2015,** *14*, 512-516; (d) Vermoortele, F.; Vandichel, M.; Van de Voorde, B.; Ameloot, R.; Waroquier, M.; Van Speybroeck, V.; De Vos, D. E. *Angew. Chem.-Int. Edit.* **2012,** *51*, 4887-4890.
21. Li, B.; Chen, D. M.; Wang, J. Q.; Yan, Z. Y.; Jiang, L.; Duan, D. L.; He, J.; Luo, Z. R.; Zhang, J. P.; Yuan, F. G. *Sci. Rep.* **2014,** *4*.
22. Furukawa, H.; Gándara, F.; Zhang, Y.-B.; Jiang, J.; Queen, W. L.; Hudson, M. R.; Yaghi, O. M. *J. Am. Chem. Soc.* **2014,** *136*, 4369-4381.
23. Delgado-Friedrichs, O.; O'Keeffe, M.; Yaghi, O. M. *Phys. Chem. Chem. Phys.* **2007,** *9*, 1035-1043.
24. Jiang, J.; Gándara, F.; Zhang, Y.-B.; Na, K.; Yaghi, O. M.; Klemperer, W. G. *J. Am. Chem. Soc.* **2014,** *136*, 12844-12847.
25. Kickelbick, G.; Wiede, P.; Schubert, U. *Inorg. Chim. Acta* **1999,** *284*, 1-7.
26. te Velde, G.; Bickelhaupt, F. M.; Baerends, E. J.; Guerra, C. F.; Van Gisbergen, S. J. A.; Snijders, J. G.; Ziegler, T. *J. Comput. Chem.* **2001,** *22*, 931-967.
27. (a) Becke, A. D. *J. Chem. Phys.* **1988,** *88*, 2547-2553; (b) Franchini, M.; Philipsen, P. H. T.; Visscher, L. *J. Comput. Chem.* **2013,** *34*, 1819-1827.
28. Becke, A. D. *Phys. Rev. A* **1988,** *38*, 3098-3100.
29. Perdew, J. P. *Phys. Rev. B* **1986,** *33*, 8822-8824.
30. Van Lenthe, E.; Baerends, E. J. *J. Comput. Chem.* **2003,** *24*, 1142-1156.
31. Lenthe, E. v.; Baerends, E. J.; Snijders, J. G. *J. Chem. Phys.* **1993,** *99*, 4597-4610.
32. Pye, C. C.; Ziegler, T. *Theor. Chem. Acc.* **1999,** *101*, 396-408.
33. Rajendiran, V.; Palaniandavar, M.; Swaminathan, P.; Uma, L. *Inorganic Chemistry* **2007,** *46*, 10446-10448.
34. Kandiah, M.; Nilsen, M. H.; Usseglio, S.; Jakobsen, S.; Olsbye, U.; Tilset, M.; Larabi, C.; Quadrelli, E. A.; Bonino, F.; Lillerud, K. P. *Chem. Mater.* **2010,** *22*, 6632-6640.
35. Plessers, E.; Fu, G.; Tan, C.; De Vos, D.; Roeffaers, M. *Catalysts* **2016,** *6*, 104.
36. Strathmann, T. J.; Myneni, S. C. B. *Geochim. Cosmochim. Acta* **2004,** *68*, 3441-3458.
37. Monera, O. D.; Sereda, T. J.; Zhou, N. E.; Kay, C. M.; Hodges, R. S. *J. Pept. Sci.* **1995,** *1*, 319-329.
38. Forbes, C. R.; Sinha, S. K.; Ganguly, H. K.; Bai, S.; Yap, G. P. A.; Patel, S.; Zondlo, N. J. *J. Am. Chem. Soc.* **2017,** *139*, 1842-1855.

39. Mondloch, J. E.; Katz, M. J.; Planas, N.; Semrouni, D.; Gagliardi, L.; Hupp, J. T.; Farha, O. K. *Chem. Commun.* **2014,** *50*, 8944-8946.
40. Wang, G.; Sharp, C.; Plonka, A. M.; Wang, Q.; Frenkel, A. I.; Guo, W.; Hill, C.; Smith, C.; Kollar, J.; Troya, D.; Morris, J. R. *J. Phys. Chem. C* **2017,** *121*, 11261-11272.
41. Poblet, J. M.; López, X., Computational Methods: Heteropolyoxoanions. In *Encyclopedia of Inorganic Chemistry*, John Wiley & Sons, Ltd: 2006.
42. Chen, Y.; Lykourinou, V.; Vetromile, C.; Hoang, T.; Ming, L.-J.; Larsen, R. W.; Ma, S. *J. Am. Chem. Soc.* **2012,** *134*, 13188-13191.

Table of Contents